Strain sensing through the resonant properties of deformed metal nanowires

Harold S. Park[a)]
Department of Mechanical Engineering, University of Colorado, Boulder, Colorado 80309, USA

(Received 29 January 2008; accepted 5 May 2008; published online 9 July 2008)

In this article, we study the potential of gold nanowires as resonant nanoscale strain sensors. The sensing ability of the nanowires is determined by calculating the variations in resonant frequency that occur due to applied uniaxial tensile and compressive strain. The resonant frequencies are obtained using the surface Cauchy–Born model, which captures surface stress effects on the nanowires through a nonlinear continuum mechanics framework; due to the continuum formulation, the strain-dependent nanowire resonant frequencies are calculated through the solution of a standard finite element eigenvalue problem, where the coupled effects of the applied uniaxial strain and surface stress are naturally included through the finite element stiffness matrix. The nanowires are found to be more sensitive to compressive than tensile strain, with resonant frequency shifts around 200–400 MHz with the application of 1% tensile and compressive strain. In general, the strain sensitivity of the nanowires is found to increase with decreasing cross-sectional size, with additional dependencies on their aspect ratio. © *2008 American Institute of Physics*.
[DOI: 10.1063/1.2953086]

I. INTRODUCTION

Nanowires are rapidly emerging as one of the basic building blocks for current and future nanoelectromechanical systems (NEMS).[1,2] The utilization of nanowires in NEMS is mainly due to their unique optical, mechanical, electrical, and thermal properties that result due to their small size.[3]

One of the areas in which nanowires are viewed as having the greatest potential is in the general arena of sensing; that is, nanowires, due to their small sizes and thus small masses in conjunction with their high stiffness, have resonant properties that are extremely sensitive to any and all environmental changes. Consequently, experiments have demonstrated the potential of nanowires at various types of sensing, including optical sensing,[4,5] chemical/biological mass sensing,[1,2,6–8] displacement sensing,[9,10] and force and strain sensing.[11,12] Furthermore, nanowires, due to their small size, can naturally operate at higher (gigahertz-range) resonant frequencies than micron-size wires can, which is critical for high-frequency sensing applications.[1]

In many of these sensing applications, the environmental change of interest is determined by measuring variations in the resonant frequencies of the nanowires. However, because the resonant frequencies of structures depend strongly upon their elastic properties, the implication is that any insightful modeling of resonance-based sensing using nanowires must accurately capture the size-dependent elastic properties of nanowires.[13–16]

The size-dependent nanowire behavior occurs because nanowires are subject to surface stresses, which arise due to the fact that atoms that lie at the surfaces of a material have fewer bonding neighbors than those that lie within the material bulk.[17,18] This disparity in bonding environment leads to surfaces having different elastic properties than the bulk; the disparity has an increasingly important effect on the effective elastic properties of the nanowires with decreasing size.[13,14,16]

The notion of mechanically tuning the resonant properties of nanowires has become reality with recent experiments that have demonstrated the ability to create variable frequency nanowire-based nanomechanical resonators through the application of tensile and compressive stress.[12,19,20] The key findings of these works are not only that the nanowire frequencies can be shifted up or down through the application of stress, but that the applied stress can be used as a tuning knob to improve the nanowire quality factors; a higher quality factor enables nanowire-based NEMS to detect ever smaller forces, masses, and environmental changes, which is critical to extending the range of application for nanowire-based resonant sensors.[2]

The purpose of this work is therefore to investigate and quantify the coupled effects of surface stresses and applied uniaxial strain on the resonant properties of gold nanowires. In particular, we seek to quantify how surface effects impact the tunability of the nanowire resonant frequencies, as this information will determine the range of applicability for nanowire-based resonant strain sensors. We accomplish this by utilizing the recently developed surface Cauchy–Born (SCB) model,[21,22] which captures nanoscale surface stress effects within a nonlinear continuum mechanics framework, to determine the resonant frequencies of gold nanowires under various degrees of uniaxial tensile and compressive strain. The SCB model is unique as compared to other surface elastic models[23–27] in that it can be utilized to capture the size-dependent mechanical behavior of surface-dominated nanomaterials such as nanowires using standard nonlinear finite element (FE) methods.[28]

The resonant frequency variations are captured naturally

[a)]Electronic mail: harold.park@colorado.edu.

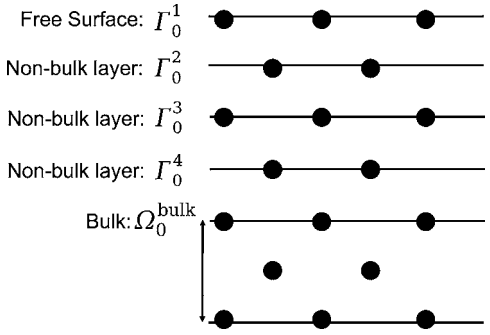

FIG. 1. Illustration of bulk and nonbulk layers of atoms in a ⟨100⟩/{100} fcc crystal interacting by an EAM potential.

through the solution of a standard eigenvalue problem using the FE method, where the FE stiffness matrix captures the coupled effects of applied strain and surface stresses on the nanowires. We quantify the strain sensitivity as functions of the nanowire surface area to volume ratio, aspect ratio, length, cross-sectional size, and the nature of the applied strain (tensile or compressive).

II. THEORY

A. Surface Cauchy–Born model

The Cauchy–Born (CB) model is a hierarchical multiscale assumption that enables the calculation of continuum stress and moduli from atomistic principles.[29] Because the CB model does not consider surface effects, the SCB model was developed[21,22] such that the energy density of a material would include contributions not only from the bulk but also the material surfaces, thus leading to the incorporation of atomistic-based surface stress effects into standard continuum stress measures.

Both the CB and SCB models are finite deformation constitutive models that exactly represent the stretching and rotation of bonds undergoing nonlinear elastic deformation through continuum mechanics-based kinematic quantities such as the deformation gradient $\mathbf{F}$, or the stretch tensor $\mathbf{C}=\mathbf{F}^T\mathbf{F}$.[28] The necessity for the finite deformation kinematics gains credence through recent work that has indicated that surface stresses can cause elastic compressive strains on the order of 1% or more in the nanowires.[22,30]

A schematic of the SCB decomposition of bulk/nonbulk atoms near a free surface is shown in Fig. 1; note that all atomic interactions involving bulk and nonbulk atoms are governed entirely by the range of the interatomic potential chosen, as would be in an atomistic simulation. Mathematically, the relationship between the continuum strain energy density and the total potential energy of the corresponding, defect-free atomistic system can be written as

$$\sum_i^{n_{\text{atoms}}} U_i(r) = \int_{\Omega_0^{\text{bulk}}} \Phi(\mathbf{C})d\Omega + \int_{\Gamma_0^1} \gamma_{\Gamma_0^1}(\mathbf{C})d\Gamma + \int_{\Gamma_0^2} \gamma_{\Gamma_0^2}(\mathbf{C})d\Gamma + \int_{\Gamma_0^3} \gamma_{\Gamma_0^3}(\mathbf{C})d\Gamma + \int_{\Gamma_0^4} \gamma_{\Gamma_0^4}(\mathbf{C})d\Gamma, \tag{1}$$

where U_i is the potential energy for atom i, r is the interatomic distance, $\Phi(\mathbf{C})$ is the bulk strain energy density, Ω_0^{bulk} represents the volume of the body in which all atoms are fully coordinated, $\gamma_{\Gamma_0^a}(\mathbf{C})$ is the surface strain energy density of a representative atom in surface layer a, and n_{atoms} is the total number of atoms in the system.

The bulk strain energy density $\Phi(\mathbf{C})$ in this work is obtained using embedded atom (EAM) potentials,[31] and takes the form

$$\Phi(\mathbf{C}) = \frac{1}{\Omega_0}[F_i(\bar{\rho}_i) + \phi_i], \tag{2}$$

$$\phi_i = \frac{1}{2}\sum_{j\neq i}^{nbrv_i} \phi_{ij}[r_{ij}(\mathbf{C})], \tag{3}$$

$$\bar{\rho}_i = \sum_{j\neq i}^{nbrv_i} \rho_j[r_{ij}(\mathbf{C})], \tag{4}$$

where $nbrv_i$ are the number of bonds in the representative unit volume Ω_0 for atom i, F_i is the embedding function, ρ_j is the contribution to the electron density at atom i from atom j, ϕ_{ij} is a pair interaction function, and r_{ij} is the distance between atoms i and j.

Analogous to the bulk energy density, the surface energy densities $\gamma(\mathbf{C})$ describe the energy per representative undeformed *area* of atoms at or near the surface of a homogeneously deforming crystal, and is also obtained using the same EAM potential as the bulk energy density. For fcc metals, choosing a surface unit cell that contains only one atom is sufficient to reproduce the structure of each surface layer. The surface unit cell possesses translational symmetry only in the plane of the surface, unlike the bulk unit cell which possesses translational symmetry in all directions. Thus, the surface energy density $\gamma\Gamma_0^a(\mathbf{C})$ for a representative atom in a given surface layer Γ_0^a in Fig. 1 can be written as

$$\gamma\Gamma_0^a(\mathbf{C}) = \frac{1}{\Gamma_0}[F_i(\bar{\rho}_i) + \phi_i], \tag{5}$$

$$\phi_i = \frac{1}{2}\sum_{j\neq i}^{nb_a} \phi_{ij}[r_{ij}(\mathbf{C})], \tag{6}$$

$$\bar{\rho}_i = \sum_{j\neq i}^{nb_a} \rho_j[r_{ij}(\mathbf{C})], \tag{7}$$

where nb_a are the number of bonds for an atom in surface layer a, and Γ_0 is the representative unit area occupied by a nonbulk atom lying at or near the free surface.

Once the bulk strain energy density is known, continuum stress measures such as the second Piola–Kirchoff stress $\mathbf{S}$ can be defined as

$$\mathbf{S} = 2\frac{\partial\Phi(\mathbf{C})}{\partial\mathbf{C}}, \tag{8}$$

while the material tangent modulus $\mathcal{C}$ is defined to be

$$\mathcal{C} = 2\frac{\partial \mathbf{S}}{\partial \mathbf{C}}. \tag{9}$$

Similarly, the surface stress on each surface layer Γ_0^a in Fig. 1 can be defined as

$$\tilde{\mathbf{S}}^{(a)}(\mathbf{C}) = 2\frac{\partial \gamma_{\Gamma_0^a}(\mathbf{C})}{\partial \mathbf{C}}, \tag{10}$$

while the surface stiffness is defined as

$$\tilde{\mathcal{C}}^{(a)}(\mathbf{C}) = 2\frac{\partial \tilde{\mathbf{S}}^{(a)}(\mathbf{C})}{\partial \mathbf{C}}. \tag{11}$$

The SCB model thus uses the surface unit cells based on the surface energies $\gamma(\mathbf{C})$ to capture the undercoordination of atoms in the surface layers. Because the surface unit cells are undercoordinated, they are not at a minimum energy, which results in the existence of surface stresses in Eq. (10) through differentiation of the surface energies $\gamma(\mathbf{C})$. As illustrated in recent atomistic[30] and SCB simulations,[22] the tensile surface stresses drive the surface atoms into the bulk such that they can increase their number of bonding neighbors and thus their electron density, leading to a more stable and lower energy configuration.

We also discuss here differences between the current formulation for surface stress, and the traditional thermodynamic definition of surface stress (see, for example Refs. 17 and 32),

$$\tau = \tau^0 + \mathbf{S}\epsilon, \tag{12}$$

where τ is the surface stress, τ^0 is the residual (strain-independent) portion of the surface stress, and $\mathbf{S}\epsilon$, where $\mathbf{S}$ is the surface elastic stiffness, is the surface-elastic (strain-dependent) part of the surface stress.

The thermodynamic interpretation of the surface stress τ in Eq. (12) is that of an excess quantity, i.e., a measure of the difference as compared to the equivalent bulk quantity. Clearly, the definition of surface stress utilized in the present work in Eq. (10) differs from Eq. (12). In particular, the surface stress defined in this work by Eq. (10) and the surface stiffness in Eq. (11) are naturally strain dependent through their dependence on the stretch tensor $\mathbf{C}$. Furthermore, no linearization is performed to obtain the surface stress or stiffness, in comparison to that used in Eq. (12)); both the surface stress in Eq. (10) and surface stiffness in Eq. (11) are fully nonlinear, finite strain-dependent quantities.

The rationale for the definition of surface stress in Eq. (10) can also be understood by analyzing the energy balance in Eq. (1). Because Eq. (1) represents the total energy of the nanostructure as decomposed into bulk and surface contributions, minimization of the energy leads directly to a force balance,[21,33] which carries the clear physical meaning that at equilibrium, the bulk forces will balance the surface forces that originate from the surface stress. Furthermore, starting from an energy balance is extremely favorable for nonlinear finite element implementation; the full details of the finite element equations is found in Park *et al.*[21] We note in closing that an extensive analysis of the SCB model in calculating the minimum energy configurations of gold nanowires as compared to benchmark atomistic calculations can be found in Park and Klein.[22]

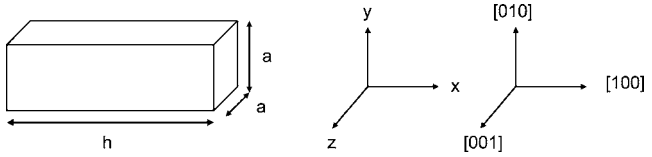

FIG. 2. Schematic of nanowire geometries considered in this work.

B. Finite element eigenvalue problem for nanowire resonant frequencies

The equation describing the eigenvalue problem for continuum elastodynamics is written as

$$(\mathbf{K} - \omega^2\mathbf{M})\mathbf{u} = 0, \tag{13}$$

where $\mathbf{M}$ is the mass matrix and $\mathbf{K}$ is the stiffness matrix of the discretized FE equations; the solution of the eigenvalue problem described in Eq. (13) gives the resonant frequencies $f = \omega/2\pi$ and the corresponding mode shapes $\mathbf{u}$. We note that the stiffness matrix $\mathbf{K}$ contains the effects of both material and geometric nonlinearities through a consistent linearization about the finitely deformed configuration.[28]

As detailed in Park and Klein,[22] once the total energy is obtained by subtracting from Eq. (1) the work due to external loads, the FE equilibrium equations can be obtained by approximating the displacement field using standard FE interpolation functions[28] and taking the first variation of the total energy.

We emphasize that the addition of the surface energy terms in Eq. (1) leads naturally to the incorporation of the surface stresses in the FE stiffness matrix $\mathbf{K}$, which then leads to the dependence of the resonant frequencies f on the surface stresses. The eigenvalue problem was solved using the Sandia-developed package TRILINOS,[34] which was incorporated into the simulation code TAHOE.[35]

III. NUMERICAL EXAMPLES

The numerical examples were performed on three-dimensional, single-crystal gold nanowires with square cross sections of width a and length h as illustrated in Fig. 2. All wires had a $\langle 100 \rangle$ axial orientation with $\{100\}$ transverse surfaces, and were fixed at both the left $(-x)$ and right $(+x)$ surfaces, similar to recent experiments utilizing strained nanowires as nanomechanical resonators.[12,19,20] Different nanowire geometries were considered to determine the effects of variations in cross-sectional area (CSA) and length on the nanowire strain sensitivity. Constant aspect ratio (AR) nanowires $(h/a = 8)$ were also considered; all geometries utilized in this work are summarized in Table I.

The SCB bulk and surface energy densities in Eqs. (2) and (5) were calculated using the Foiles EAM potential for gold.[36] The bulk FE stresses were calculated using Eq. (8) while the surface FE stresses were found using Eq. (10). All SCB calculations utilized regular meshes of 8-node hexahe-

TABLE I. Summary of nanowire geometries considered: constant aspect ratio (AR), constant length, and constant cross-sectional area (CSA). All dimensions are in nanometers.

Constant AR	Constant length	Constant CSA
$96\times12\times12$	$160\times12\times12$	$128\times16\times16$
$144\times18\times18$	$160\times18\times18$	$192\times16\times16$
$192\times24\times24$	$160\times24\times24$	$256\times16\times16$

dral finite elements; FE mesh sizes ranging from 13 000 to 71 000 nodes were used to model the nanowire geometries.

The calculation of the resonant frequencies under strain were performed as follows. Initially, the nanowires are out of equilibrium due to the surface stresses;[22,37] therefore, the fixed/fixed nanowires were allowed to first relax to an energy minimizing configuration under the influence of surface stresses. We note that the nanowires are in a state of tensile stress at the minimum energy configuration; the reason for this is that the nanowires would, without constraint, contract axially due to surface stresses to reduce their transverse surface area.[37–39] Previous research has illustrated the ability of the SCB model to accurately capture deformation arising solely due to surface stresses as compared to benchmark atomistic calculations.[22]

However, the fixed end boundary conditions prevent the contraction from occurring, and thus the nanowires exist in a tensile stress state. To illustrate the accuracy of the SCB model for the fixed/fixed boundary conditions that are utilized in this work, a comparison between the SCB model (576 finite elements) and a fully atomistic molecular statics calculation (145 000 atoms) of the minimum energy configuration (at zero percent applied strain) for a $25\times10\times10$ nm fixed/fixed nanowire is shown in Fig. 3. The resonant frequencies calculated for this minimum energy configuration (without imposed strain, but accounting for surface stress effects) are labeled f_0 in the subsequent figures and discussion.

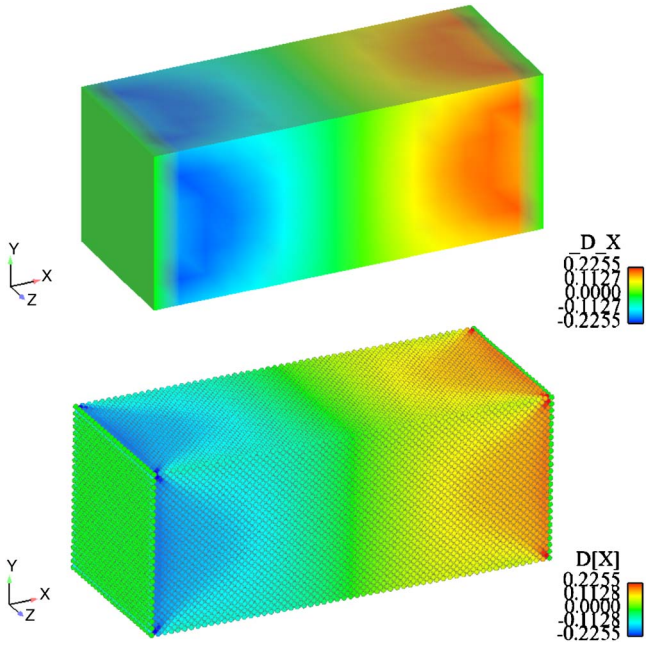

FIG. 3. (Color online) Comparison of (top) SCB and (bottom) molecular statics calculations of the minimum energy configuration of $25\times10\times10$ nm fixed/fixed gold nanowire under the influence of surface stresses.

These nonzero stress minimum energy configurations were chosen instead of starting from zero stress configurations due to the recent experimental works of Verbridge *et al.*,[12,19] who found that prestressing silicon carbide nanowires under tension leads to enhanced quality factors, which are necessary in resonant sensing applications to enhance sensitivity to nanoscale forces, masses, and strains. Therefore, in the present work we utilize the fact that the fixed/fixed boundary conditions in conjunction with the surface stresses naturally lead to an effectively tensile prestress in the nanowires.

From this reference configuration, the nanowires were subjected to either uniaxial tensile or compressive strain by elongating one end of the nanowire through a fixed displacement boundary condition. The strain in both tension and compression was applied in ten loading increments of $\epsilon=\pm0.1\%$ such that a final state of 1% strain in both tension and compression was reached. After each increment of strain was applied, the nanowire was allowed to relax to an energy minimizing configuration. At that point, the fundamental resonant frequency was calculated through solution of the FE eigenvalue problem detailed in Eq. (13); the shifts in resonant frequency occur due to the variation in the stiffness $\mathbf{K}$ resulting from the tensile or compressive state of deformation of the nanowire coupled with the surface stress effects.

To quantify the effects of the surface stresses on the resonant frequencies, resonant frequencies were also performed using the bulk CB (BCB) model,[29] which does not account for surface stresses. In other words, the energy density considered for the BCB model contains only the bulk strain energy $\Phi(\mathbf{C})$ in Eq. (1), and neglects the surface energy densities $\gamma(\mathbf{C})$. In the subsequent discussion, we compare the resonant frequencies due to surface stresses as calculated using the SCB model against the frequencies obtained using the BCB model to quantify the effects of surface stresses and applied strain on the nanowire resonant frequencies.

A. Constant cross-sectional area nanowires

The first set of results for the resonant frequencies of nanowires under strain was obtained for the case in which the nanowire CSA was kept constant with a width of $a=16$ nm as seen in Table I, leading to aspect ratios of $h/a=8$, 12, and 16.

We first show in Fig. 4 the resonant frequencies for both the SCB and BCB models with $h/a=16$ as a function of strain. As would be expected, both the SCB and BCB frequencies increase with applied tensile strain,[40] and decrease with applied compressive strain, with the BCB results showing a larger decrease in resonant frequency with increasing compressive strain. The SCB frequencies are larger in all cases considered because the nanowire is initially in a tensile state of stress due to the surface stresses, as shown in Fig. 3, which is a check on the qualitative nature of the SCB solutions.

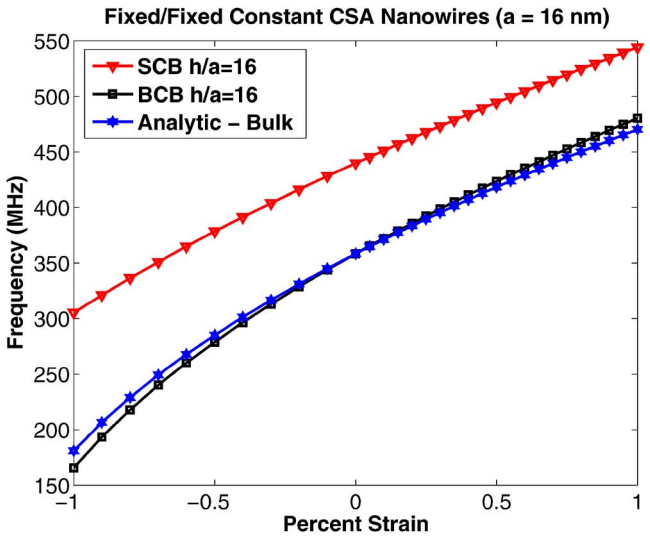

FIG. 4. (Color online) SCB and BCB predictions of the resonant frequencies of constant cross-sectional area nanowires ($h/a=16$) as a function of strain as compared to analytic solution in Eq. (14).

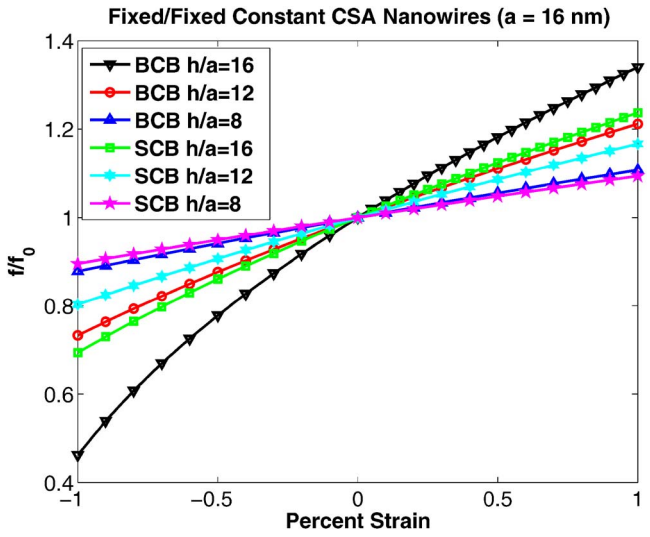

FIG. 5. (Color online) SCB and BCB predictions of the normalized resonant frequencies of constant cross-sectional area gold nanowires as a function of strain.

Figure 4 also plots the resonant frequencies as compared to an analytic formula derived by Cao *et al.*[41] for the resonant frequency of a fixed/fixed carbon nanotube (CNT) for a given strain ϵ from continuum beam theory. With minor modifications to account for the fact that nanowires have a different geometry than nanotubes, the frequency shift due to strain can be expressed as

$$f_\epsilon - f_0 = \frac{i^2\pi}{2h^2}\sqrt{\frac{EI}{\rho A}}\left(\sqrt{1+\epsilon\frac{Ah^2}{4\pi^2 I}}-1\right), \tag{14}$$

where f_0 is the zero strain resonant frequency, f_ϵ is the resonant frequency at strain ϵ, i is a geometric constant, where $i\approx 1.5$ for fixed/fixed beams, I is the moment of inertia, A is the cross-sectional area, h is the length of the beam, ρ is the density, and E is the Young's modulus.

As can be observed in Fig. 4, the analytic solution and the BCB solution match extremely well, with an overprediction by the SCB solution that occurs due to the fact that the nanowires are in tension as the fixed end boundary conditions prevent contraction due to surface stresses. However, it is observed that there is a deviation between the BCB and analytic solutions as the applied strain becomes large, or on the order of about 0.2% in both tension and compression. This occurs because the BCB model is a finite deformation, nonlinearly elastic constitutive model, in which the stiffness of the material is not constant with deformation as is assumed in Eq. (14), and in which the geometry (i.e., the cross-sectional area and length) is also not constant due to deformation. Thus, the analytic solution in Eq. (14) begins to underpredict the resonant frequencies at finite strain due to the fact that nonlinear effects are not accounted for.

Figure 5 illustrates the variation in the normalized resonant frequencies for both BCB and SCB results for the constant CSA nanowires under tensile and compressive strain, where the frequencies for both were normalized by their zero strain frequency f_0. An interesting trend that is observed in Fig. 5 that is also observed for the other parametric studies conducted is that, while the SCB resonant frequencies are always larger for a given geometry than the BCB frequencies, the variation in the SCB resonant frequencies is always less than the variation in the BCB resonant frequencies as a function of both tensile and compressive strain.

The SCB nanowires exhibit a smaller variation in resonant frequencies with applied strain due to the fact that the nanowires are initially in a state of tensile stress that places the nanowire behavior in the nonlinear elastic regime. Therefore, the SCB nanowires show a reduction in stiffness with increasing strain, which reduces the strain sensitivity as compared to the BCB nanowires.

In all cases for the SCB nanowires as shown in Fig. 6, the strain sensitivity is greater in compression than tension. For the $h/a=16$ SCB nanowire, the resonant frequency shift at 1% compression is 134 MHz, while the frequency shift at 1% tension is 104 MHz. The strain sensitivity is larger for

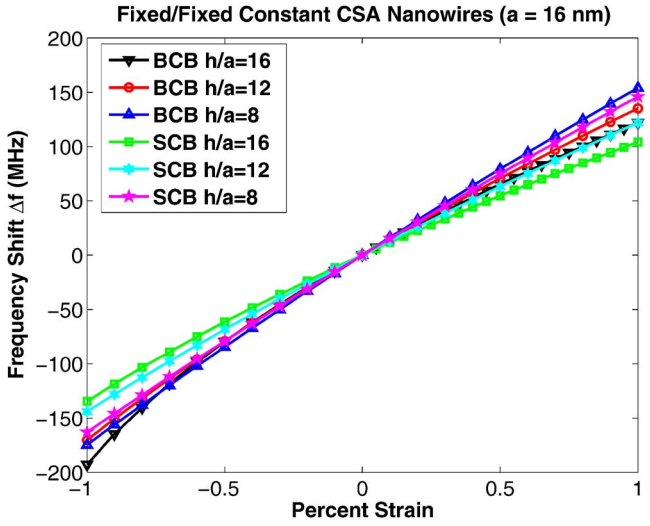

FIG. 6. (Color online) SCB and BCB predictions of the strain sensitivity of constant cross-sectional area nanowires.

TABLE II. BCB and SCB predictions of the total strain sensitivity (difference in resonant frequency between 1% compressive strain and 1% tensile strain) of constant CSA nanowires. Dimensions in nanometers, total strain sensitivity in megahertz.

Geometry	BCB	SCB
128×16×16	328.81	308.96
192×16×16	305.55	265.89
256×16×16	314.80	238.75

the smaller aspect ratios; for the $h/a=8$ SCB nanowire, the frequency shift is 163 MHz at 1% compression, and 146 MHz at 1% tension.

This is further quantified in Table II, which quantifies the overall strain sensitivities of the nanowires through a measure we call the total strain sensitivity. The strain sensitivity is an important parameter as it measures the change in resonant frequency that occurs for a given increment of strain; we define the total strain sensitivity to be the difference between the resonant frequency at 1% tensile strain and at 1% compressive strain. Table II shows that the largest strain sensitivity occurs for both SCB and BCB nanowires for the smallest aspect ratio ($h/a=8$) nanowires, with total strain sensitivities exceeding 300 MHz in both the SCB and BCB cases; the strain sensitivity is observed to decrease for increasing aspect ratio h/a.

B. Constant length nanowires

The results for the constant length nanowires under imposed uniaxial strain are shown in Figs. 7 and 8. As in the constant CSA case, the nanowires show an increase in resonant frequency with increasing tensile strain, while showing a decrease in resonant frequency with increasing compressive strain. Also of interest as shown in Fig. 7, the nanowires exhibit similar trends in normalized resonant frequency shift as a function of h/a with respect to the initial configuration, as did the constant CSA nanowires in Fig. 5.

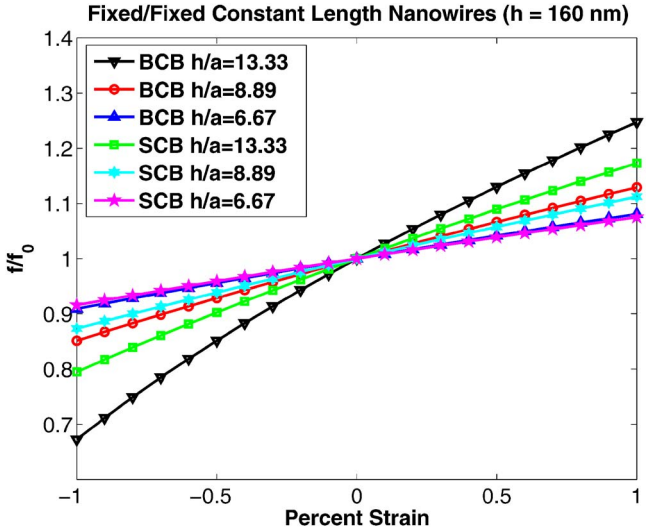

FIG. 7. (Color online) SCB and BCB predictions of the normalized resonant frequencies of constant length nanowires as a function of strain.

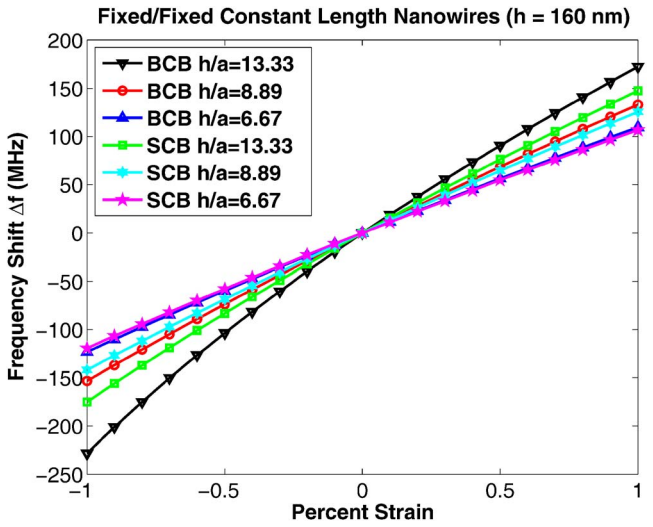

FIG. 8. (Color online) SCB and BCB predictions of the strain sensitivity of constant length nanowires.

Figure 8 and Table III illustrate the total strain sensitivity of the constant length nanowires. For the constant length case, both the SCB and BCB nanowires are observed to show an increase in total strain sensitivity with a decrease in cross-sectional area, or increasing h/a, which differs from the constant CSA nanowires. For the 24 nm cross section, the SCB nanowires exhibit a total strain sensitivity of 226 MHz, while halving the cross-sectional length to 12 nm increases the total strain sensitivity to 322 MHz. In contrast, the BCB nanowires at 24 nm have a total strain sensitivity of 233 MHz, with an increase to a total strain sensitivity of 400 MHz at 12 nm.

The SCB constant length nanowires also show greater strain sensitivity in compression than tension, with the difference increasing with increasing aspect ratio. For example, the 12 nm cross-section SCB nanowire has a resonant frequency shift of 175 MHz at 1% compression, and 147 MHz at 1% tension. In comparison, the 24 nm cross-ection SCB nanowire has a resonant frequency shift of 119 MHz at 1% compression, and 107 MHz at 1% tension.

C. Constant aspect ratio nanowires

Finally, we discuss the resonant frequencies for the constant aspect ratio (AR) nanowires under strain to augment and clarify the size-dependent results that were found for the constant length nanowires; the results are summarized in Figs. 9 and 10. Again, as shown in Fig. 9, the constant AR nanowires follow the trends observed for the constant CSA

TABLE III. BCB and SCB predictions of the total strain sensitivity (difference in resonant frequency between 1% compressive strain and 1% tensile strain) of constant length nanowires. Dimensions in nanometers, total strain sensitivity in megahertz.

Geometry	BCB	SCB
160×12×12	400.78	322.43
160×18×18	286.20	267.35
160×24×24	232.60	225.78

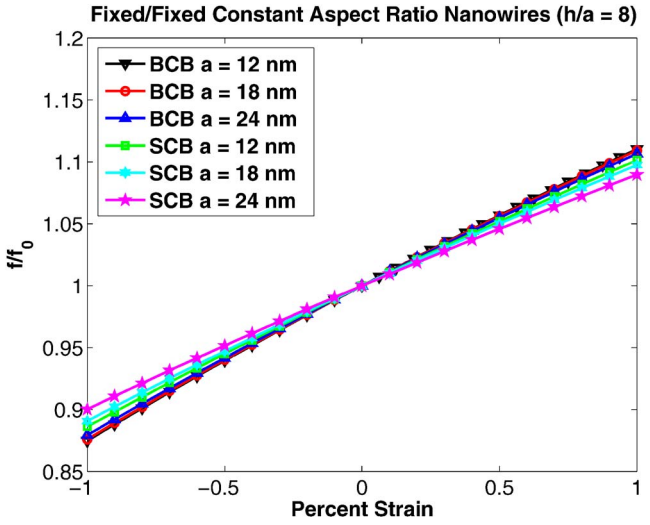

FIG. 9. (Color online) SCB and BCB predictions of the normalized resonant frequencies of constant aspect ratio nanowires as a function of strain.

and length nanowires in that the normalized resonant frequencies increase in tension, and decrease in compression. It is interesting to find that, despite having the same AR, the nanowires exhibit large differences between their resonant frequencies as a function of strain. In addition, similar to previous cases, the constant AR nanowires show greater strain sensitivity in compression than tension.

Figure 10 and Table IV show the total strain sensitivity for the constant AR nanowires. As can be seen, though the aspect ratio is kept constant at $h/a=8$, the strain sensitivity for the SCB nanowires clearly increases with a decrease in cross-sectional size; the total strain sensitivity is reduced by nearly 50% from 403 to 214 MHz by doubling the cross-sectional length from 12 to 24 nm. These results in conjunction with those found for the constant length nanowires clearly indicate the gain in sensing performance, i.e., an increase in the total strain sensitivity, that may be exploited by simply decreasing the size of the nanowires.

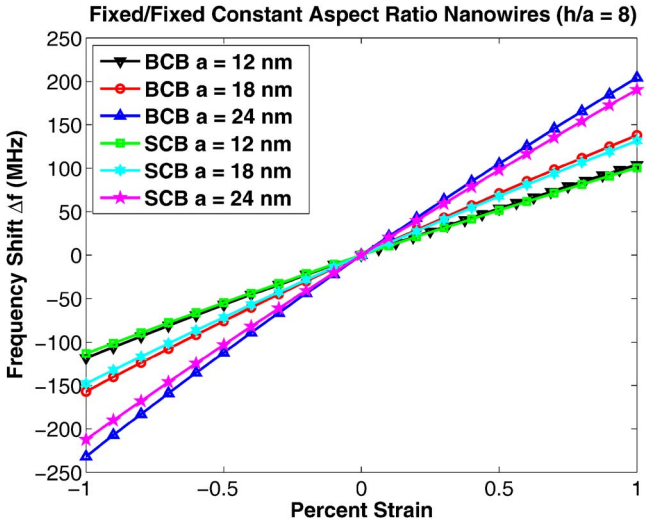

FIG. 10. (Color online) SCB and BCB predictions of the resonant frequency shift of constant aspect ratio nanowires due to applied strain.

TABLE IV. BCB and SCB predictions of the total strain sensitivity (difference in resonant frequency between 1% compressive strain and 1% tensile strain) of constant aspect ratio nanowires. Dimensions in nanometers, total strain sensitivity in megahertz.

Geometry	BCB	SCB
$96\times12\times12$	436.41	403.07
$144\times18\times18$	295.02	279.78
$192\times24\times24$	222.38	213.63

D. Discussion

After having presented the results from all three parametric studies, we have found information to assist in the design of highly strain sensitive nanowires. In general, smaller cross sections (for a given nanowire length or aspect ratio) and smaller aspect ratios (for a given nanowire cross section) appear to lead to greater total strain sensitivity. We additionally quantify a potential design variable that appears to hold constant over all cases; that is, all nanowires appear to be more sensitive to compressive strain than tensile strain. This is quantified in Fig. 11, which plots the ratio of the frequency shift at 1% compressive strain to that at 1% tensile strain for all three geometry types (constant CSA, AR, length) for the SCB nanowires, i.e., when surface stresses are accounted for; we note that similar trends are found for the BCB nanowires.

We also plot in Fig. 11 the results for constant surface area to volume (SAV) ratio nanowires, which varied in cross-sectional size from 14.7 to 15.2 nm while having lengths that ranged from 110 to 230 nm; the surface area to volume ratio was kept constant at 0.28 nm^{-1}. As can be seen, Fig. 11 shows that for the constant CSA, length, and SAV nanowires, the selective strain sensitivity of nanowires to compression can be increased dramatically by increasing the nanowire aspect ratio h/a. Also of interest, Fig. 11 shows that, for the constant AR nanowires, the selective strain sensitivity to compression remains relatively constant (around 1.12 times)

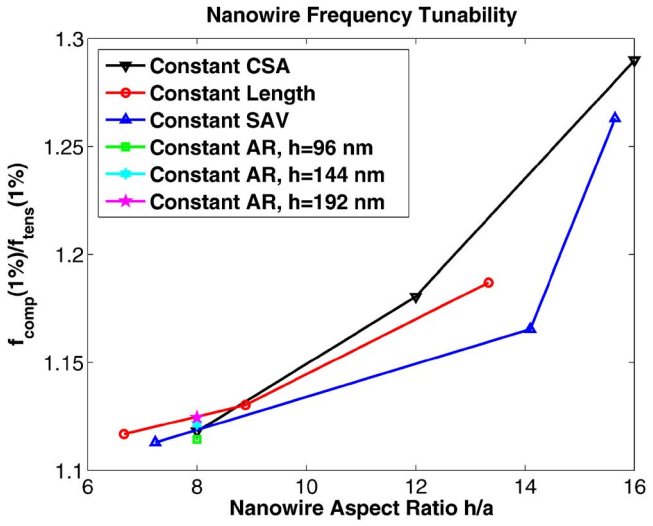

FIG. 11. (Color online) Ratio of the frequency shift at 1% compressive strain to that at 1% tensile strain vs the nanowire aspect ratio h/a for SCB nanowires.

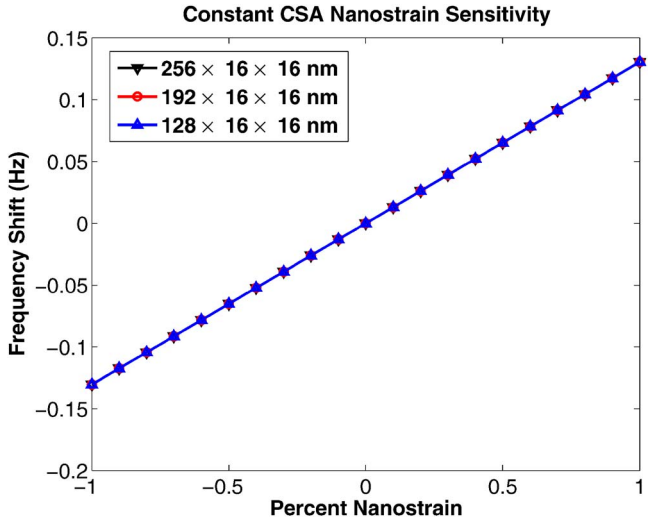

FIG. 12. (Color online) Beam theory prediction based on Eq. (14) of the effects of axial nanostrain on the fundamental resonant frequency of a gold nanowire.

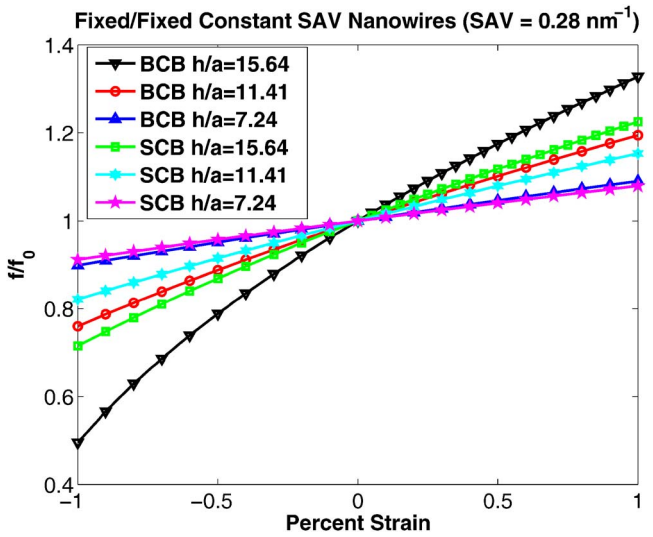

FIG. 13. (Color online) SCB and BCB predictions of the normalized resonant frequencies of constant SAV nanowires as a function of strain.

despite the doubling in cross-sectional dimension, though a small increase is found with increasing cross-sectional dimension.

We also quantify the potential of nanowires as ultrasensitive strain sensors, similar to that done by Cao *et al.*,[41] and Li and Chou,[42] calculating the strain sensitivity of the nanowires at the level of nanostrain, or $\epsilon = 10^{-11}$. The nanostrain sensitivity is calculated using Eq. (14) for the constant CSA nanowires considered in this work, with the results plotted in Fig. 12. As shown, gold nanowires with the dimensions analyzed in this work have a nanostrain sensitivity on the order of 0.1 Hz, with the strain sensitivity increasing with decreasing cross-sectional area. Thus, so long as the experimental equipment that is being used to detect the resonant frequency has a sensitivity of about 0.01 Hz, gold nanowires may be used as nanoscale strain sensors.

The present results for gold nanowires can be compared with existing results for the strain sensitivity of CNTs.[41,42] In comparison, the CNTs have a nanostrain sensitivity on the order of kilohertz as compared to hertz for the nanowires, with the likely reason for this being the fact that the CNT modulus is on the order of TPa, while the ⟨100⟩ nanowire modulus is on the order of 36 GPa.

We also discuss the present results in the context of the recent experimental work of Verbridge *et al.*,[12,19] who studied the effects of applied stress on the resonant frequencies and quality factors of 100 nm cross-section silicon nitride and single-crystal silicon nanowires. While frequency sensitivity as a function of strain was not explicitly given in that work, the largest frequency shift that was obtained due to stress was about 40 MHz. If the dimensions of the nanowires considered in this work are increased by an order of magnitude to match those in the Verbridge work (for example making the $192 \times 16 \times 16$ nm wire in this work a $1920 \times 16 \times 16$ nm nanowire), we find that the total strain sensitivity would be about 30 MHz, which is comparable to that found experimentally.

We also discuss the lack of surface area to volume ratio dependence on the strain sensitivity that is found in this work. To further elaborate this point, we plot in Fig. 13 the variation in normalized resonant frequencies for the constant SAV nanowires considered in this work. It would appear from the similarities between Figs. 5, 7, and 13 that the normalized resonant frequencies of nanowires under uniaxial strain are strongly dependent on the aspect ratio h/a, while showing little to no dependence on SAV. Indeed, these results correlate with the fact that no dependence of the strain sensitivity on the surface area to volume ratio has been found experimentally.[12]

IV. CONCLUSIONS

The purpose of this work has been to perform a detailed study as to the coupled effects of surface stresses and applied uniaxial deformation on the resonant frequencies and thus the strain sensitivity of gold nanowires. This was accomplished by utilizing the SCB model[21,22] to study the effects of uniaxial tensile and compressive strain on the fundamental resonant frequency of gold nanowires at zero temperature. Because it captures nanoscale surface stress effects within a continuum mechanics framework, the SCB model can be efficiently utilized to predict the resonant properties of the nanowires through the solution of a standard FE eigenvalue problem with a full accounting of the surface stress effects and applied strain through the FE stiffness matrix; such calculations would be nearly intractable using fully atomistic calculations.

By subjecting gold nanowires of various geometry (constant cross-sectional area, length, surface area to volume ratio, and aspect ratio) to uniaxial tensile and compressive strain, we draw the following conclusions: (1) The resonant frequencies of the nanowires increase with tensile strain and decrease with compressive strain. (2) The nanowires were shown to have a strain sensitivity on the order of 0.01 Hz at the level of nanostrains. (3) For design purposes, we find that nanowires with smaller aspect ratios (for a given cross-

sectional size) or smaller cross-sectional sizes (for a given length or aspect ratio) are more sensitive to changes in strain. These findings have positive ramifications for strain-sensitive nanowire-based NEMS, in that they imply that decreasing the nanowire size leads to significant improvements in strain sensitivity. (4) The total strain sensitivity, measured by the difference in resonant frequency at 1% compressive and 1% tensile strain, was found to be on the order of 200–400 MHz for the nanowire sizes considered in this work. (5) The nanowires were found in all cases to be more sensitive to compressive as compared to tensile strain. Furthermore, the relative sensitivity to compression can be increased for all nanowire geometries considered simply by increasing the nanowire aspect ratio. (6) The major effect of surface stresses is to reduce the total strain sensitivity of the nanowires as compared to the corresponding bulk material.

ACKNOWLEDGMENTS

H.S.P. gratefully acknowledges NSF Grant Number CMMI-0750395 in support of this research.

[1]H. G. Craighead, Science **290**, 1532 (2000).
[2]K. L. Ekinci and M. L. Roukes, Rev. Sci. Instrum. **76**, 061101 (2005).
[3]Y. Xia, P. Yang, Y. Sun, Y. Wu, B. Mayers, B. Gates, Y. Yin, F. Kim, and H. Yan, Adv. Mater. **15**, 353 (2003).
[4]J. Lou, L. Tong, and Z. Ye, Opt. Express **13**, 2135 (2005).
[5]D. J. Sirbuly, M. Law, P. Pauzauskie, H. Yan, A. V. Maslov, K. Knutsen, C.-Z. Ning, R. J. Saykally, and P. Yang, Proc. Natl. Acad. Sci. U.S.A. **102**, 7800 (2005).
[6]M. Law, J. Goldberger, and P. Yang, Annu. Rev. Mater. Res. **34**, 83 (2004).
[7]J. Fritz, M. K. Baller, H. P. Lang, H. Rothuizen, P. Vettiger, E. Meyer, H. J. Guntherodt, C. Gerber, and J. K. Gimzewski, Science **288**, 316 (2000).
[8]G. Y. Chen, T. Thundat, E. A. Wachter, and R. J. Warmack, J. Appl. Phys. **77**, 3618 (1995).
[9]A. N. Cleland, J. S. Aldridge, D. C. Driscoll, and A. C. Gossard, Appl. Phys. Lett. **81**, 1699 (2002).
[10]K. L. Ekinci, Small **1**, 786 (2005).
[11]T. D. Stowe, K. Yasumura, T. W. Kenny, D. Botkin, K. Wago, and D. Rugar, Appl. Phys. Lett. **71**, 288 (1997).
[12]S. S. Verbridge, J. M. Parpia, R. B. Reichenbach, L. M. Bellan, and H. G. Craighead, J. Appl. Phys. **99**, 124304 (2006).
[13]E. W. Wong, P. E. Sheehan, and C. M. Lieber, Science **277**, 1971 (1997).
[14]S. Cuenot, C. Frétigny, S. Demoustier-Champagne, and B. Nysten, Phys. Rev. B **69**, 165410 (2004).
[15]B. Wu, A. Heidelberg, and J. J. Boland, Nat. Mater. **4**, 525 (2005).
[16]G. Y. Jing, H. L. Duan, X. M. Sun, Z. S. Zhang, J. Xu, Y. D. Li, J. X. Wang, and D. P. Yu, Phys. Rev. B **73**, 235409 (2006).
[17]R. C. Cammarata, Prog. Surf. Sci. **46**, 1 (1994).
[18]W. Haiss, Rep. Prog. Phys. **64**, 591 (2001).
[19]S. S. Verbridge, D. F. Shapiro, H. G. Craighead, and J. M. Parpia, Nano Lett. **7**, 1728 (2007).
[20]V. Cimalla, C. Foerster, F. Will, K. Tonisch, K. Brueckner, R. Stephan, M. E. Hein, O. Ambacher, and E. Aperathitis, Appl. Phys. Lett. **88**, 253501 (2006).
[21]H. S. Park, P. A. Klein, and G. J. Wagner, Int. J. Numer. Methods Eng. **68**, 1072 (2006).
[22]H. S. Park and P. A. Klein, Phys. Rev. B **75**, 085408 (2007).
[23]P. Lu, H. P. Lee, C. Lu, and S. J. O'Shea, Phys. Rev. B **72**, 085405 (2005).
[24]M. E. Gurtin, X. Markenscoff, and R. N. Thurston, Appl. Phys. Lett. **29**, 529 (1976).
[25]J. E. Sader, J. Appl. Phys. **89**, 2911 (2001).
[26]G. Y. Huang, W. Gao, and S. W. Yu, Appl. Phys. Lett. **89**, 043506 (2006).
[27]A. W. McFarland, M. A. Poggi, M. J. Doyle, L. A. Bottomley, and J. S. Colton, Appl. Phys. Lett. **87**, 053505 (2005).
[28]T. Belytschko, W. K. Liu, and B. Moran, *Nonlinear Finite Elements for Continua and Structures* (John Wiley and Sons, New York, 2002).
[29]E. Tadmor, M. Ortiz, and R. Phillips, Philos. Mag. A **73**, 1529 (1996).
[30]H. Liang, M. Upmanyu, and H. Huang, Phys. Rev. B **71**, 241403(R) (2005).
[31]M. S. Daw and M. I. Baskes, Phys. Rev. B **29**, 6443 (1984).
[32]V. B. Shenoy, Phys. Rev. B **71**, 094104 (2005).
[33]Z. P. Huang and J. Wang, Acta Mech. **182**, 195 (2006).
[34]TRILINOS, http://software.sandia.gov/trilinos/index.html (2007).
[35]TAHOE, http://tahoe.ca.sandia.gov (2007).
[36]S. M. Foiles, M. I. Baskes, and M. S. Daw, Phys. Rev. B **33**, 7983 (1986).
[37]J. Diao, K. Gall, and M. L. Dunn, Nat. Mater. **2**, 656 (2003).
[38]H. S. Park, K. Gall, and J. A. Zimmerman, Phys. Rev. Lett. **95**, 255504 (2005).
[39]W. Liang, M. Zhou, and F. Ke, Nano Lett. **5**, 2039 (2005).
[40]W. Weaver, S. P. Timoshenko, and D. H. Young, *Vibration Problems in Engineering* (John Wiley and Sons, New York, 1990).
[41]G. Cao, X. Chen, and J. W. Kysar, Phys. Rev. B **72**, 195412 (2005).
[42]C.-Y. Li and T.-W. Chou, Nanotechnology **15**, 1493 (2004).